

Electrical Control of Interband Resonant Nonlinear Optics in Monolayer MoS₂

*Yunyun Dai, * † Yadong Wang, † Susobhan Das, † Hui Xue, † Xueyin Bai, † Eero Hulkko, †*

*Guangyu Zhang, ‡ Xiaoxia Yang, § Qing Dai, § and Zhipei Sun * †, #*

†Department of Electronics and Nanoengineering, Aalto University, Fi-00076 Aalto, Finland

‡Institute of Physics and Beijing National Laboratory for Condensed Matter Physics, Chinese
Academy of Sciences, Beijing 100190, China

§Division of Nanophotonics, CAS Center for Excellence in Nanoscience, National Center for
Nanoscience and Technology, Beijing 100190, China

#QTF Centre of Excellence, Department of Applied Physics, Aalto University, Fi-00076
Aalto, Finland

*Email: yunyun.dai@aalto.fi, zhipei.sun@aalto.fi

ABSTRACT: Monolayer transition metal dichalcogenides show strong optical nonlinearity with great potential for various emerging applications. Here, we demonstrate the gate-tunable interband resonant four-wave mixing and sum-frequency generation in monolayer MoS₂. Up to 80% modulation depth in four-wave mixing is achieved when the generated signal is resonant with A-exciton at room temperature, corresponding to an effective third-order optical nonlinearity $|\chi^{(3)}_{\text{eff}}|$ tuning from ~ 12.0 to $5.45 \times 10^{-18} \text{ m}^2/\text{V}^2$. The tunability of the effective second-order optical nonlinearity $|\chi^{(2)}_{\text{eff}}|$ at 440 nm C-exciton resonance wavelength is also demonstrated from ~ 11.6 to $7.40 \times 10^{-9} \text{ m/V}$ with sum-frequency generation. Such large tunability in optical nonlinearities arises from the strong excitonic charging effect in monolayer transition metal dichalcogenides, which allows for electrical control of the interband excitonic transitions and thus nonlinear optical responses for future on-chip nonlinear optoelectronics.

KEYWORDS: nonlinear optics, four-wave mixing, sum-frequency generation, gate-tunability, exciton, MoS₂

Atomically thin transition metal dichalcogenides (TMDs) have stimulated great interest due to their favorable physical properties,^{1, 2} such as extremely large exciton binding energy,³ and valley pseudospin physics arising from a large spin-orbit interaction.⁴ Particularly, TMD monolayers feature a direct bandgap in the visible spectral range,^{2, 5} enabling diverse photonic applications including modulators,⁶ photodetectors,⁷ and light-emitting diodes.⁸ Furthermore, TMD monolayers have recently attracted a surge of attention focusing on their fascinating optical nonlinearities⁹ (e.g., harmonic generation¹⁰⁻¹² and saturable absorption^{13, 14}), promising

for various applications,¹⁵ such as wavelength conversion^{16, 17} and ultrafast pulse generation.¹⁸⁻²⁰

In TMD monolayers, the strongly bound and tunable excitons^{3, 21, 22} enable the enhanced light-matter interaction^{23, 24} and tunable linear and nonlinear optical responses at the atomic thickness scale.^{25, 26} For example, it has been demonstrated that the strong interband excitonic effect results in the significant enhancement of various harmonic generation processes^{27, 28} in TMD monolayers. Additionally, it has been reported that second-harmonic generation in WSe₂ monolayer can be electrically tuned at A-exciton resonance.²⁶ The interband excitonic enhancement and tunability of nonlinear optical (NLO) responses are fascinating for numerous applications and will enable the versatility of future modern photonics, which is challenging with traditional NLO materials.^{26, 29-31} However, the electrical control of the other NLO responses in TMDs still remains unexplored, although it is highly desired for future applications.

In this work, we report the interband excitonic effect of various nonlinear optical processes, including four-wave mixing (FWM) and sum-frequency generation (SFG), in monolayer MoS₂ at room temperature. We fabricate an ion-gel gated monolayer MoS₂ device for effective electron doping by applying positive gate voltages. We demonstrate the excitonic enhancement and the gate-tunable FWM of monolayer MoS₂. Similarly, for the SFG process, the enhancement and the nonlinear optical tunability at the interband excitonic resonance are also reported. Besides, the second- and third-order nonlinear coefficients are calculated as a function of doping carrier densities.

RESULTS AND DISCUSSION

Linear optical characterization in monolayer MoS₂. A schematic and an optical image of the MoS₂ device are shown in Figure 1a, b. The device consists of a chemical vapor

deposited (CVD) monolayer MoS₂ sheet on a SiO₂/Si substrate, with Ti/Au (5/50 nm) as the source and drain electrodes. The ion-gel top gate method³² is used for electrostatic gating, which changes the doping level and therefore the optical responses of MoS₂. By examining Raman and photoluminescence spectra (Figure S1 in Supporting Information), the CVD MoS₂ film is identified as a monolayer. Here, the electrical property of the monolayer MoS₂ is measured with different gate voltages. The transport curve is characteristic of an *n*-type semiconductor, as shown in Figure 1b. Over a gate voltage range (-3V to 3V), the source-drain current increases with positive gating (*i.e.*, $V_g > 0.4$ V), indicating effectively electron-injection to MoS₂. The low off-current is due to the MoS₂-contact Schottky barrier.³³ Note that, in our experimental range (*i.e.*, the gate voltage range is between -3 and 3 V), we are not able to obtain effective hole doping. Therefore, in the following experiments, we mainly study the device at positive gating with effective electron doping.

In order to understand the excitonic effect on linear optical properties, the reflection spectra of the MoS₂ device are measured with electron doping at positive gating. The linear absorption spectrum of monolayer MoS₂ on a reference sapphire substrate shows pronounced absorption peaks attributed to A (~650 nm), B (~610 nm) and C (~440 nm) excitonic transitions with no electrostatic gating (grey curve in Figure 1c). However, at a large gate-voltage (*e.g.*, $V_g = 3$ V with doping carrier density of $\sim 4 \times 10^{13} / \text{cm}^2$), the excitonic effect is strongly suppressed (Supporting Information Figure S2a). The carrier density is estimated using the capacitor model $N = C(V_g - V_{\text{on}})/e$, in which C is the ion-gel capacitance 2.45 $\mu\text{F}/\text{cm}^2$, e is the elementary charge, and $V_{\text{on}} = 0.4$ V is the turn-on voltage in the monolayer MoS₂ device³². Here, we plot the differential reflection spectra $\frac{R(V_g) - R(3V)}{R(3V)}$ in Figure 1c, where $R(V_g)$ represents the reflection of the monolayer MoS₂ film on the Si/SiO₂ substrate at V_g . The differential reflection spectra clearly show a gate-tunable linear optical response at A and B

excitons. This is mainly because the injected carriers (*e.g.*, electrons when $V_g > 0.4$ V) decrease the oscillator strength of interband excitonic transitions.²⁵ The higher the positive gate voltage is, the weaker the excitonic transitions induced linear absorption will be. And with high enough gate-voltage (*e.g.*, $V_g = 3$ V), the interband excitonic transitions could even be switched off, while a lower-energy resonance known as trion (*e.g.*, A-) emerges (Figure S2b in Supporting Information).³⁴ The trion (A-) resonance is quite weak, which is observable only by the derivative of the reflection spectra. Therefore, the influence of trion is insignificant in our experiments at room temperature. Note that negligible change is observed at C exciton, which is consistent with the result discussed in Ref. 25.

Gate-control of interband resonant FWM in MoS₂. A home-built femtosecond laser based microscopic system (Figure S3a in Supporting Information) is employed for the nonlinear optical measurements in monolayer MoS₂, as described in Methods. The monolayer MoS₂ film, excited by two pump frequencies at ω_1 and ω_2 ($\omega_1 > \omega_2$), typically generates various nonlinear optical signals, *e.g.*, second-harmonic signals ($2\omega_1$ and $2\omega_2$), SFG signal ($\omega_1 + \omega_2$), and FWM ($2\omega_1 \pm \omega_2$, $\omega_1 \pm 2\omega_2$), as shown in Supporting Information Figure S4.

Here, we mainly study the FWM generation (inset of Figure 2a): pump light ($\hbar\omega_1$) is fixed at ~ 1.55 eV (*i.e.*, $\lambda_1 = \sim 800$ nm) and idler light ($\hbar\omega_2$) is tunable in a near-infrared spectral range from ~ 1.1 to 1.33 eV (*i.e.*, $\lambda_2 = \sim 930 - 1120$ nm). As a result, wavelength-dependent FWM ($\omega_{\text{FWM}} = 2\omega_1 - \omega_2$) from ~ 1.77 to 2.00 eV (*i.e.*, $\lambda_{\text{FWM}} = \sim 620 - 700$ nm) is studied as shown in Figure 2a. The average power for both pump and idler input light beams in the experiment is $\sim 1\mu\text{W}$ (with a corresponding peak intensity of ~ 44 GW/cm²). We find that the FWM is enhanced at around 650 nm, when the generated FWM photon energy (*i.e.*, $\hbar\omega_{\text{FWM}} = \sim 1.91$ eV) matches the A-excitonic energy of monolayer MoS₂, suggesting the interband resonance at A-exciton (Figure 2b).

We further study the interband resonant FWM at A-exciton. Here, we use pump light ($\hbar\omega_1$) at ~ 1.55 eV (*i.e.*, $\lambda_1 = \sim 800$ nm) and idler light ($\hbar\omega_2$) at ~ 1.19 eV (*i.e.*, $\lambda_2 = \sim 1040$ nm), and the generated FWM ($\omega_{\text{FWM}} = 2\omega_1 - \omega_2$) is at ~ 1.91 eV (*i.e.*, $\lambda_{\text{FWM}} = \sim 650$ nm). To examine the power dependence of the resonant FWM signal, the nonlinear optical spectra are measured when the power of pump (P_1) and idler (P_2) light beams is changed, respectively. The upper panel of Figure 2c shows the peak intensities of the FWM spectra with increasing P_1 while $P_2 = 1 \mu\text{W}$. The lower panel of Figure 2c shows the peak intensities of FWM spectra with increasing P_2 while $P_1 = 1 \mu\text{W}$. It roughly follows a square and linear power law behavior as a function of P_1 and P_2 , respectively, which confirms the two-color FWM process ($\omega_{\text{FWM}} = 2\omega_1 - \omega_2$) involving the pump and idler light beams (details in Supporting Information). We also study the gate-tunable resonant FWM in monolayer MoS₂ with interband A-excitonic resonance, as shown in Figure 2d. The FWM intensities decrease significantly when V_g changes from 0 to 3 V. We attribute the gate tunable FWM to the modulation of oscillator strength of interband excitonic resonance by the gate injected electrons.²⁶ With increasing gate voltages, the oscillator strength at the excitonic resonance decreases with increased doping (as shown in Figure 1c), thus suppressing the exciton enhancement of nonlinear processes.²⁶ As a result, the FWM signals decrease with increasing gate voltage at the excitonic resonant wavelength. Note that the gate tunable FWM results are repeatable (Figure S5 in Supporting Information).

Similarly, with pump light ($\hbar\omega_1$) at ~ 1.55 eV (*i.e.*, $\lambda_1 = \sim 800$ nm) and idler light ($\hbar\omega_2$) at ~ 1.07 eV (*i.e.*, $\lambda_2 = \sim 1160$ nm), the generated FWM ($\omega_{\text{FWM}} = 2\omega_1 - \omega_2$) at ~ 2.03 eV (*i.e.*, $\lambda_{\text{FWM}} = \sim 610$ nm) is resonant with B-excitonic state. Figure 2e shows gate-tunable resonant FWM spectra at B-exciton, where the FWM intensities also decrease with increased electrostatic doping due to the same operation principle.

The normalized gate-tunable FWM ($\frac{I_{\text{FWM}}(V_g)}{I_{\text{FWM}}(0 \text{ V})}$) is plotted in Figure 2f, where $I_{\text{FWM}}(V_g)$ is the peak intensity of FWM at V_g . Here, we achieve a nearly 80% (70%) modulation depth ($\frac{|I_{\text{FWM}}(V_g) - I_{\text{FWM}}(0 \text{ V})|}{I_{\text{FWM}}(0 \text{ V})}$) when FWM is resonant at A(B)-excitonic states with V_g tuning from 0 to 3 V. As a comparison, for the FWM at 700 nm (*i.e.*, λ_1 at 800 nm and λ_2 at 920 nm), which is off excitonic resonance, gating does not change the FWM intensity (black dots in Figure 2f). This further demonstrates the dominance of the interband excitonic effect on the optical nonlinearity of monolayer TMDs. Note that the FWM remains constant when $V_g < \sim 0.4$ V, which is due to that the effective electron injection to MoS₂ has a turn-on threshold V_{on} at 0.4 V. This critical V_{on} is also indicated by the transport characteristics of monolayer MoS₂ (Figure 1b).

Gate-control of interband resonant SFG in MoS₂. We also use the home-built femtosecond laser based microscopic system to study SFG in monolayer MoS₂, as described in Methods. The SFG at the sum frequency ($\omega_{\text{SFG}} = \omega_1 + \omega_2$) is generated with the two input light beams at ω_1 and ω_2 . In our SFG experiment, pump1 ($\hbar\omega_1$) is fixed at ~ 1.55 eV (*i.e.*, $\lambda_1 = \sim 800$ nm) and pump2 ($\hbar\omega_2$) is tunable in the near-infrared spectral range from ~ 1.11 to 1.33 eV (*i.e.*, $\lambda_2 = \sim 930 - 1120$ nm). As a result, wavelength-dependent SFG is achieved from ~ 2.66 to 2.88 eV (*i.e.*, $\lambda_{\text{SFG}} = \sim 430 - 465$ nm) (Figure 3a). We find that SFG is enhanced at around 440 nm, when the generated SFG photon energy (*i.e.*, $\hbar\omega_{\text{SFG}} = \sim 2.82$ eV) matches the C-excitonic energy of monolayer MoS₂ (the inset of Figure 3a). The enhancement suggests that interband excitonic transition at C-exciton significantly contributes to the enhanced SFG process. The power dependent SFG signals are examined (Figure 3b). The peak intensities of the SFG spectra scale linearly with pump1 power P_1

(while pump2 power $P_2 = \sim 1 \mu\text{W}$) and P_2 (while $P_1 = \sim 1 \mu\text{W}$), respectively, following the linear power law behavior of SFG.

We also study the gate-tunable SFG of MoS₂ with interband C-excitonic resonance. The peak intensities of the resonant SFG at 440 nm decrease with increased electrostatic doping (Figure 3c), showing a nearly 60% modulation depth ($\frac{|I_{\text{SFG}}(V_g) - I_{\text{SFG}}(0 \text{ V})|}{I_{\text{SFG}}(0 \text{ V})}$) at $V_g = 3 \text{ V}$, where $I_{\text{SFG}}(V_g)$ is the peak intensity of SFG at V_g . This demonstrates gate-tunability of the SFG process in monolayer MoS₂.

Gate-tunable nonlinear optical coefficients. We have realized the tunability of nonlinear optical signals, which arises from the strong excitonic charging effects in monolayer MoS₂, allowing for exceptional control over the oscillator strengths at the excitonic resonances. Based on the measured tunable FWM and SFG intensities, we can estimate the tunability of nonlinear coefficients of MoS₂. The second- and third-order nonlinear coefficients $\chi^{(2)}$ and $\chi^{(3)}$ are calculated from the measured average powers of the incident light and the generated nonlinear optical signals as follows,³⁵

$$|\chi^{(2)}| = \frac{8n_s c}{\alpha_s \omega_s} \sqrt{\frac{\varphi f \tau_1 \tau_2 D_1^2 D_2^2 n_1 n_2 \varepsilon_0 c P_s}{\tau_s D_s^2 n_s P_1 P_2}}, \quad (1)$$

$$|\chi^{(3)}| = \frac{8n_F c}{\alpha_F \omega_F} \frac{\varphi f \tau_1 D_1^2 n_1 \varepsilon_0 c}{P_1} \sqrt{\frac{\tau_2 D_2^2 n_2 P_F}{\tau_F D_F^2 n_F P_2}}, \quad (2)$$

where $P_{(1,2,S,F)}$ are the average powers of the two incident pump beams and generated SFG/FWM signals, and $f = 2 \text{ kHz}$ is the repetition rate, and $\tau_{(1,2,S,F)} = \sim 230 \text{ fs}$ is the estimated pulse duration of pump light beams and SFG/FWM signals, and $D_{(1,2,S,F)} = \sim 2.5 \mu\text{m}$ is the diameter of the Gaussian spatial profile on the sample, and $n_{(1,2,S,F)} = \sim 4.2$ is refractive index of the material at the pump light frequencies and SFG/FWM frequencies²⁵, and $\alpha_S = 2$ for two-color SFG process, $\alpha_F = 3$ for two-color FWM process, and $\varphi = (\pi/\ln 2)^{3/2}/8$. Therefore, the effective bulk-like second- and third-order nonlinear coefficients of monolayer MoS₂

$(\chi^{(2)\text{eff}}, \chi^{(3)\text{eff}})$ can be obtained, $\chi^{(2)\text{eff}} = \chi^{(2)}/t$ and $\chi^{(3)\text{eff}} = \chi^{(3)}/t$, where $t = \sim 0.7$ nm is the thickness of monolayer MoS₂. The detailed calibration and calculation method are discussed in Supporting Information. The typical average power of two pump light beams is ~ 1 μW for each light beam. When the gate voltage varies from 0 to 3 V, corresponding to carrier density change from 0 to $\sim 4 \times 10^{13}$ /cm², the SFG signal at C-exciton is changing from ~ 2.5 to 1.0 pW, and the FWM signal is changing from ~ 0.14 to 0.029 pW at A-exciton, and from ~ 0.093 to 0.028 pW at B-exciton. Therefore, we obtain the gate-tunable $|\chi^{(2)\text{eff}}|$ and $|\chi^{(3)\text{eff}}|$ of monolayer MoS₂, as shown in Figure 4. The tunability of $|\chi^{(3)\text{eff}}|$ changes from $\sim 12.0 - 5.45 \times 10^{-18}$ m²/V² at interband A-excitonic resonance ($\sim 9.16 - 5.03 \times 10^{-18}$ m²/V² at interband B-excitonic resonance) as a function of doping carrier density (Figure 4a). Similarly, the tunability of $|\chi^{(2)\text{eff}}|$ with interband C-exciton resonance at 440 nm changes from $\sim 11.6 - 7.40 \times 10^{-9}$ m/V with varying the doping carrier density (Figure 4b).

The calculated second and third-order nonlinear coefficients $|\chi^{(2)\text{eff}}|$ and $|\chi^{(3)\text{eff}}|$ are of the order of 10^{-9} m/V and 10^{-18} m²/V², which are in the same range of previously reported work (e.g., $|\chi^{(2)\text{eff}}| = \sim 5 \times 10^{-9}$ m/V in Ref. 36; $|\chi^{(3)\text{eff}}| = \sim 10^{-17} - 10^{-19}$ m²/V² in Ref. 12). Besides the electrical tunability, different approaches have been developed to tune nonlinear optical responses of TMDs. For example, strain^{37, 38} and plasmonic antenna³⁹ induced tunability of nonlinear optical response has been studied in TMDs (fully discussed in Supporting Information). For further improvement, integrating monolayer MoS₂ with waveguides,⁴⁰ optical fibers,⁴¹ or optical cavities³¹ will enhance light-matter interactions for higher light conversion efficiency. Besides, gate-tunable optical nonlinearity at low temperature offers the possibility for higher tunability and better understanding of the underlying physics.²⁶

CONCLUSIONS

To conclude, the interband excitonic resonance of FWM and SFG is investigated in ion-gel gated monolayer MoS₂ at room temperature. The gate-tunable interband excitonic FWM and SFG are demonstrated by electrostatic doping, which originates from the modulation of oscillator strength of interband excitonic resonances. For interband resonant FWM, $|\chi^{(3)\text{eff}}|$ of monolayer MoS₂ changes from $\sim 12.0 - 5.45 \times 10^{-18} \text{ m}^2/\text{V}^2$ at A-exciton (650 nm), and from $\sim 9.16 - 5.03 \times 10^{-18} \text{ m}^2/\text{V}^2$ at B-exciton (610 nm). Similarly, the tunability of $|\chi^{(2)\text{eff}}|$ with interband C-exciton resonance at 440 nm is tuned from $\sim 11.6 - 7.40 \times 10^{-9} \text{ m/V}$ with gate voltage varying from 0 to 3 V. Note that the similar nonlinear optical tunability is anticipated to other TMDs (*e.g.*, WS₂). Therefore, our study is promising for electrically-controlled NLO devices based on two-dimensional layered materials (*e.g.*, tunable saturable absorbers,⁴² on-chip nonlinear optics⁴³), extending the versatility of modern photonic systems.

METHODS

MoS₂ device fabrication. The monolayer MoS₂ is grown on a SiO₂/Si substrate by CVD method.⁴⁴ The source, drain and gate electrodes were first patterned using electron-beam lithography (Vistec) and then deposited with Ti/Au (5/50 nm) using electron-beam evaporation. All the electrodes were wire-bonded to a chip for electrical control. Ion-gel was spin-coated uniformly on the MoS₂ device. The ion-gel solution was prepared by dissolving 22 mg of poly(styrene)-*b*-poly(ethylene oxide)-*b*-poly(styrene) (PS-PEO-PS) and 0.56 g of ion liquid ([EMIM][TFSI]) in 20 ml of anhydrous dichloromethane.³² The ion liquid and dry dichloromethane were purchased from Sigma Aldrich, and PS-PEO-PS was purchased from Polymer Source.

Nonlinear optical spectra measurement. A home-built femtosecond laser based microscopic system is employed for the nonlinear optical experiments. The schematic of this system is shown in Figure S3a in Supporting Information. Two incident light beams, with

different frequencies, are linearly polarized with polarization directions parallel with each other. Their typical spectra are shown in Supporting Information Figure S3b. The pulse duration of the incident pulses is ~230 fs, which is estimated by the cross-correlation measurement (Figure S3c in Supporting Information). The pulses of the two pump light beams are spatially and temporally overlapped, focused collinearly on the sample and generate the nonlinear optical signals in the monolayer MoS₂ film. The spectra of nonlinear optical signals are detected by a spectrometer (Andor, Hamamatsu) in the reflection configuration. The nonlinear optical signals of the monolayer MoS₂ were measured under different gate voltages. Note that when different source-drain voltages were applied, no change was observed in nonlinear optical signals. Therefore, to fully exclude electric current-induced nonlinear optical effects (*e.g.*, current-induced second-order nonlinearity⁴⁵), we only apply gate voltage and ground source and drain electrodes (*i.e.*, no source-drain current) in our experiments.

ASSOCIATED CONTENT

Supporting Information. MoS₂ film characterization, gate-tunable electrical and linear optical properties of monolayer MoS₂, FWM and SFG experiment setup and spectra of pump light, nonlinear optical spectra in monolayer MoS₂, the repeatable gate-tunable FWM, gate-tunable SFG spectra with excitonic resonance and off-resonance, calculation of nonlinear coefficients for SFG and FWM signals in MoS₂, and wavelength-dependent third-order nonlinear coefficients of monolayer MoS₂, comparison among different tuning approaches

This material is available free of charge *via* the Internet at <http://pubs.acs.org>.

AUTHOR INFORMATION

Corresponding Author

*E-mail: Yunyun.dai@aalto.fi.

*E-mail: zhipei.sun@aalto.fi.

ORCID

Zhipei Sun: 0000-0002-9771-5293

Yunyun Dai: 0000-0002-1186-1864

Yadong Wang: 0000-0001-8603-3468

Author Contributions

Y.D. and Z.S. conceived the idea. Y. D. performed the measurements with assistance from Y. W., S. D., H. X., X. B., and E. H. on the device preparation and gate-tunable optical measurements. G. Z., X. Y., and Q. D. provided the CVD-grown MoS₂ sample. Y. D. analysed the experimental data. Y. D. and Z. S wrote the manuscript with contributions from all authors.

Notes

The authors declare no competing financial interest.

ACKNOWLEDGEMENT

The authors thank funding from Aalto Centre for Quantum Engineering, Business Finland (A-Photonics), Academy of Finland (Grant Nos. 276376, 284548, 295777, 304666, 312297, 312551, and 314810), Academy of Finland Flagship Programme (Grant No. 320167, PREIN), the European Union's Horizon 2020 research and innovation program (Grant No. 820423, S2QUIP), and ERC (Grant No. 834742).

REFERENCES

- (1) Manzeli, S.; Ovchinnikov, D.; Pasquier, D.; Yazyev, O. V.; Kis, A. 2D Transition Metal Dichalcogenides. *Nat. Rev. Mater.* **2017**, 2, 17033.

(2) Mak, K. F.; Lee, C.; Hone, J.; Shan, J.; Heinz, T. F. Atomically Thin MoS₂: a New Direct-Gap Semiconductor. *Phys. Rev. Lett.* **2010**, *105*, 136805.

(3) He, K.; Kumar, N.; Zhao, L.; Wang, Z.; Mak, K. F.; Zhao, H.; Shan, J. Tightly Bound Excitons in Monolayer WSe₂. *Phys. Rev. Lett.* **2014**, *113*, 026803.

(4) Xu, X.; Yao, W.; Xiao, D.; Heinz, T. F. Spin and Pseudospins in Layered Transition Metal Dichalcogenides. *Nat. Phys.* **2014**, *10*, 343-350.

(5) Splendiani, A.; Sun, L.; Zhang, Y.; Li, T.; Kim, J.; Chim, C. Y.; Galli, G.; Wang, F. Emerging Photoluminescence in Monolayer MoS₂. *Nano Lett.* **2010**, *10*, 1271-5.

(6) Sun, Z.; Martinez, A.; Wang, F. Optical Modulators with 2D Layered Materials. *Nat. Photon.* **2016**, *10*, 227-238.

(7) Lopez-Sanchez, O.; Lembke, D.; Kayci, M.; Radenovic, A.; Kis, A. Ultrasensitive Photodetectors Based on Monolayer MoS₂. *Nat. Nanotechnol.* **2013**, *8*, 497-501.

(8) Sundaram, R. S.; Engel, M.; Lombardo, A.; Krupke, R.; Ferrari, A. C.; Avouris, P.; Steiner, M. Electroluminescence in Single Layer MoS₂. *Nano Lett.* **2013**, *13*, 1416-21.

(9) Autere, A.; Jussila, H.; Dai, Y.; Wang, Y.; Lipsanen, H.; Sun, Z. Nonlinear Optics with 2D Layered Materials. *Adv. Mater.* **2018**, *30*, e1705963.

(10) Autere, A.; Jussila, H.; Marini, A.; Saavedra, J. R. M.; Dai, Y.; Säynätjoki, A.; Karvonen, L.; Yang, H.; Amirsolaimani, B.; Norwood, R. A.; Peyghambarian, N.; Lipsanen, H.; Kieu, K.; de Abajo, F. J. G.; Sun, Z. Optical Harmonic Generation in Monolayer Group-VI Transition Metal Dichalcogenides. *Phys. Rev. B* **2018**, *98*, 115426.

(11) Karvonen, L.; Säynätjoki, A.; Huttunen, M. J.; Autere, A.; Amirsolaimani, B.; Li, S.; Norwood, R. A.; Peyghambarian, N.; Lipsanen, H.; Eda, G.; Kieu, K.; Sun, Z. Rapid

Visualization of Grain Boundaries in Monolayer MoS₂ by Multiphoton Microscopy. *Nat. Commun.* **2017**, *8*, 15714.

(12) Saynatjoki, A.; Karvonen, L.; Rostami, H.; Autere, A.; Mehravar, S.; Lombardo, A.; Norwood, R. A.; Hasan, T.; Peyghambarian, N.; Lipsanen, H.; Kieu, K.; Ferrari, A. C.; Polini, M.; Sun, Z. Ultra-Strong Nonlinear Optical Processes and Trigonal Warping in MoS₂ Layers. *Nat. Commun.* **2017**, *8* (1), 893.

(13) Yan, P.; Chen, H.; Yin, J.; Xu, Z.; Li, J.; Jiang, Z.; Zhang, W.; Wang, J.; Li, I. L.; Sun, Z.; Ruan, S. Large-Area Tungsten Disulfide for Ultrafast Photonics. *Nanoscale* **2017**, *9*, 1871-1877.

(14) Chen, H.; Yin, J.; Yang, J.; Zhang, X.; Liu, M.; Jiang, Z.; Wang, J.; Sun, Z.; Guo, T.; Liu, W.; Yan, P. Transition-Metal Dichalcogenides Heterostructure Saturable Absorbers for Ultrafast Photonics. *Opt. Lett.* **2017**, *42*, 4279-4282.

(15) Wang, Q. H.; Kalantar-Zadeh, K.; Kis, A.; Coleman, J. N.; Strano, M. S. Electronics and Optoelectronics of Two-dimensional Transition Metal Dichalcogenides. *Nat. Nanotechnol.* **2012**, *7*, 699-712.

(16) Li, D.; Xiong, W.; Jiang, L.; Xiao, Z.; Golgor, H. R.; Wang, M.; Huang, X.; Zhou, Y.; Lin, Z.; Song, J.; Ducharme, S.; Jiang, L.; Silvain, J. F.; Lu, Y. Multimodal Nonlinear Optical Imaging of MoS₂ and MoS₂-Based van der Waals Heterostructures. *ACS Nano* **2016**, *10*, 3766-75.

(17) Jakubczyk, T.; Delmonte, V.; Koperski, M.; Nogajewski, K.; Faugeras, C.; Langbein, W.; Potemski, M.; Kasprzak, J. Radiatively Limited Dephasing and Exciton Dynamics in MoSe₂ Monolayers Revealed with Four-Wave Mixing Microscopy. *Nano Lett.* **2016**, *16*, 5333-9.

(18) Mao, D.; Wang, Y.; Ma, C.; Han, L.; Jiang, B.; Gan, X.; Hua, S.; Zhang, W.; Mei, T.; Zhao, J. WS₂ Mode-Locked Ultrafast Fiber Laser. *Sci. Rep.* **2015**, *5*, 7965.

(19) Bonaccorso, F.; Sun, Z. Solution Processing of Graphene, Topological Insulators and Other 2D Crystals for Ultrafast Photonics. *Opt. Mater. Express* **2013**, *4*, 63-78.

(20) Zhang, H.; Bao, Q.; Sun, Z. Introduction to Two-Dimensional Layered Materials for Ultrafast Lasers. *Photon. Research* **2018**, *6*, TDL1-TDL2.

(21) Ugeda, M. M.; Bradley, A. J.; Shi, S. F.; da Jornada, F. H.; Zhang, Y.; Qiu, D. Y.; Ruan, W.; Mo, S. K.; Hussain, Z.; Shen, Z. X.; Wang, F.; Louie, S. G.; Crommie, M. F. Giant Bandgap Renormalization and Excitonic Effects in a Monolayer Transition Metal Dichalcogenide Semiconductor. *Nat. Mater.* **2014**, *13*, 1091-5.

(22) Chernikov, A.; van der Zande, A. M.; Hill, H. M.; Rigosi, A. F.; Velauthapillai, A.; Hone, J.; Heinz, T. F. Electrical Tuning of Exciton Binding Energies in Monolayer WS₂. *Phys. Rev. Lett.* **2015**, *115*, 126802.

(23) Suri, G.; Zhou, Y.; High, A. A.; Wild, D. S.; Shu, C.; De Greve, K.; Jauregui, L. A.; Taniguchi, T.; Watanabe, K.; Kim, P.; Lukin, M. D.; Park, H. Large Excitonic Reflectivity of Monolayer MoSe₂ Encapsulated in Hexagonal Boron Nitride. *Phys. Rev. Lett.* **2018**, *120*, 037402.

(24) Malard, L. M.; Alencar, T. V.; Barboza, A. P. M.; Mak, K. F.; de Paula, A. M. Observation of Intense Second Harmonic Generation from MoS₂ Atomic Crystals. *Phys. Rev. B* **2013**, *87*, 201401.

(25) Yu, Y.; Yu, Y.; Huang, L.; Peng, H.; Xiong, L.; Cao, L. Giant Gating Tunability of Optical Refractive Index in Transition Metal Dichalcogenide Monolayers. *Nano Lett.* **2017**, *17*, 3613-3618.

(26) Seyler, K. L.; Schaibley, J. R.; Gong, P.; Rivera, P.; Jones, A. M.; Wu, S.; Yan, J.; Mandrus, D. G.; Yao, W.; Xu, X. Electrical Control of Second-Harmonic Generation in a WSe₂ Monolayer Transistor. *Nat. Nanotechnol.* **2015**, *10*, 407-11.

(27) Wang, G.; Marie, X.; Gerber, I.; Amand, T.; Lagarde, D.; Bouet, L.; Vidal, M.; Balocchi, A.; Urbaszek, B. Giant Enhancement of the Optical Second-Harmonic Emission of WSe₂ Monolayers by Laser Excitation at Exciton Resonances. *Phys. Rev. Lett.* **2015**, *114*, 097403.

(28) Yoshikawa, N.; Nagai, K.; Uchida, K.; Takaguchi, Y.; Sasaki, S.; Miyata, Y.; Tanaka, K. Interband Resonant High-Harmonic Generation by Valley Polarized Electron-Hole Pairs. *Nat. Commun.* **2019**, *10*, 3709.

(29) Jiang, T.; Huang, D.; Cheng, J.; Fan, X.; Zhang, Z.; Shan, Y.; Yi, Y.; Dai, Y.; Shi, L.; Liu, K.; Zeng, C.; Zi, J.; Sipe, J. E.; Shen, Y.-R.; Liu, W.-T.; Wu, S. Gate-Tunable Third-Order Nonlinear Optical Response of Massless Dirac Fermions in Graphene. *Nat. Photon.* **2018**, *12*, 430-436.

(30) Soavi, G.; Wang, G.; Rostami, H.; Purdie, D. G.; De Fazio, D.; Ma, T.; Luo, B.; Wang, J.; Ott, A. K.; Yoon, D.; Bourelle, S. A.; Muench, J. E.; Goykhman, I.; Dal Conte, S.; Celebrano, M.; Tomadin, A.; Polini, M.; Cerullo, G.; Ferrari, A. C. Broadband, Electrically Tunable Third-Harmonic Generation in Graphene. *Nat. Nanotechnol.* **2018**, *13*, 583-588.

(31) Zhipei, S. Electrically Tuned Nonlinearity. *Nat. Photon.* **2018**, *12*, 383-385.

(32) Chen, C. F.; Park, C. H.; Boudouris, B. W.; Horng, J.; Geng, B.; Girit, C.; Zettl, A.; Crommie, M. F.; Segalman, R. A.; Louie, S. G.; Wang, F. Controlling Inelastic Light Scattering Quantum Pathways in Graphene. *Nature* **2011**, *471*, 617-20.

(33) Kaushik, N.; Nipane, A.; Basheer, F.; Dubey, S.; Grover, S.; Deshmukh, M. M.; Lodha, S. Schottky Barrier Heights for Au and Pd Contacts to MoS₂. *Appl. Phys. Lett.* **2014**, *105*, 113505.

(34) Mak, K. F.; He, K.; Lee, C.; Lee, G. H.; Hone, J.; Heinz, T. F.; Shan, J. Tightly Bound Trions in Monolayer MoS₂. *Nat. Mater.* **2012**, *12*, 207-211.

(35) Boyd, R. W. The Nonlinear Optical Susceptibility. *Nonlinear Optics*, 3rd Edition; Academic Press: New York, 2008.

(36) Kumar, N.; Najmaei, S.; Cui, Q.; Ceballos, F.; Ajayan, P. M.; Lou, J.; Zhao, H. Second-Harmonic Microscopy of Monolayer MoS₂. *Phys. Rev. B* **2013**, *87*, 161403.

(37) Liang, J.; Wang, J.; Zhang, Z.; Su, Y.; Guo, Y.; Qiao, R.; Song, P.; Gao, P.; Zhao, Y.; Jiao, Q.; Wu, S.; Sun, Z.; Yu, D.; Liu, K. Universal Imaging of Full Strain Tensor in 2D Crystals with Third-Harmonic Generation. *Adv. Mater.* **2019**, *31*, e1808160.

(38) Liang, J.; Zhang, J.; Li, Z.; Hong, H.; Wang, J.; Zhang, Z.; Zhou, X.; Qiao, R.; Xu, J.; Gao, P.; Liu, Z.; Liu, Z.; Sun, Z.; Meng, S.; Liu, K.; Yu, D. Monitoring Local Strain Vector in Atomic-Layered MoSe₂ by Second-Harmonic Generation. *Nano Lett.* **2017**, *17*, 7539-7543.

(39) Li, J.; Ji, Q.; Chu, S.; Zhang, Y.; Li, Y.; Gong, Q.; Liu, K.; Shi, K. Tuning the Photo-Response in Monolayer MoS₂ by Plasmonic Nano-Antenna. *Sci. Rep.* **2016**, *6*, 23626.

(40) Alexander, K.; Savostianova, N. A.; Mikhailov, S. A.; Kuyken, B.; Van Thourhout, D. Electrically Tunable Optical Nonlinearities in Graphene-Covered SiN Waveguides Characterized by Four-Wave Mixing. *ACS Photonics* **2017**, *4*, 3039-3044.

(41) Chen, K.; Zhou, X.; Cheng, X.; Qiao, R.; Cheng, Y.; Liu, C.; Xie, Y.; Yu, W.; Yao, F.; Sun, Z.; Wang, F.; Liu, K.; Liu, Z. Graphene Photonic Crystal Fibre with Strong and Tunable Light–Matter Interaction. *Nat. Photon.* **2019**, *13*, 754-759.

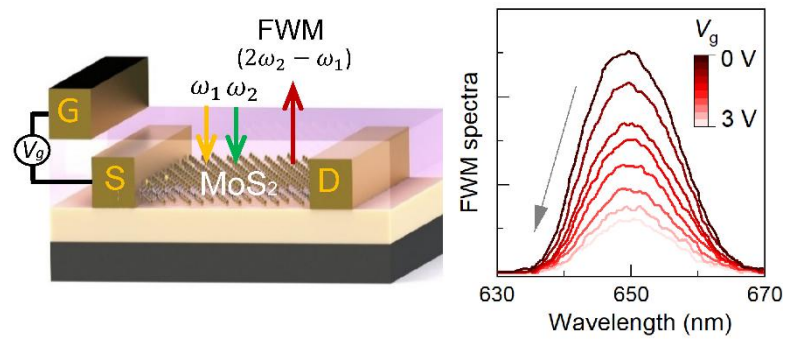
(42) Bonaccorso, F.; Sun, Z.; Hasan, T.; Ferrari, A. C. Graphene Photonics and Optoelectronics. *Nat. Photon.* **2010**, *4*, 611-622.

(43) Ferrari, A. C.; Bonaccorso, F.; Fal'ko, V.; Novoselov, K. S.; Roche, S.; Boggild, P.; Borini, S.; Koppens, F. H.; Palermo, V.; Pugno, N.; Garrido, J. A.; Sordan R.; Bianco A.; Ballerini L.; Prato M.; Lidorikis E.; Kivioja J.; Marinelli C.; Ryhänen T.; Morpurgo A.; *et al.* Science and Technology Roadmap for Graphene, Related Two-Dimensional Crystals, and Hybrid Systems. *Nanoscale* **2015**, *7*, 4598-810.

(44) Chen, W.; Zhao, J.; Zhang, J.; Gu, L.; Yang, Z.; Li, X.; Yu, H.; Zhu, X.; Yang, R.; Shi, D.; Lin, X.; Guo, J.; Bai, X.; Zhang, G. Oxygen-Assisted Chemical Vapor Deposition Growth of Large Single-Crystal and High-Quality Monolayer MoS₂. *J. Am. Chem. Soc.* **2015**, *137*, 15632-5.

(45) An, Y. Q.; Nelson, F.; Lee, J. U.; Diebold, A. C. Enhanced Optical Second-Harmonic Generation from the Current-Biased Graphene/SiO₂/Si(001) Structure. *Nano Lett.* **2013**, *13*, 2104-9.

SYNOPSIS TOC



For Table of Contents Only